Optimal Control of the Plasma Azimuthal Velocity Profile by Feedback $E \times B$ Actuation in HELCAT

Zeki Okan Ilhan, David Huxley-Cohen, Hexiang Wang, Eugenio Schuster, Mark Gilmore, and Andrew Ware

***Abstract*— Active control of the flow shear, which is related to the radial derivative of the azimuthal flow, is a key factor in reducing the cross-field turbulence-driven particle transport in a magnetically confined plasma column. Once a desired radial azimuthal velocity profile and its associated level of turbulent fluctuations are identified, the challenge of systematically achieving and sustaining it still remains. In this paper, a model-based feedback controller is proposed to overcome this challenge in helicon-cathode (HELCAT). This linear, dual-source, magnetized-plasma, laboratory device employs concentric ring electrodes to mitigate the turbulent plasma transport by generating a sheared radial electric field and modifying the flow profiles by $E \times B$ actuation. A linear-quadratic-integral optimal feedback controller is designed to minimize a weighted combination of the tracking error and the control effort with an ultimate goal of regulating the radial azimuthal velocity profile around a prescribed desired profile even with external disturbances and perturbed initial conditions. Numerical simulations show the effectiveness of the proposed controller in shaping the azimuthal flow profile in HELCAT. The proposed control solution has the potential of being used as a systematic tool for physics-oriented studies in laboratory plasmas such as those achieved in HELCAT.**

***Index Terms*— Azimuthal velocity profile control, optimal linear-quadratic-integral feedback control, plasma transport control.**

I. Introduction

NOWADAYS, laboratory plasma physics has found applications in various research areas ranging from solar corona heating and laboratory astrophysics to plasma nonlinear dynamics and turbulence control mechanisms. Plasma experiments in such wide range of application areas need a plasma source that can generate a broad plasma parameter space with a plasma duration of several milliseconds [1]. Therefore, the HELCAT dual-source linear plasma device, which utilizes both helicon and thermionic cathode sources, has been created. The helicon plasmas are characterized by their high density, relatively longer discharge times, and peaked profiles, whereas the cathode plasmas typically have lower density, short discharge time, and broader profiles. Combining the two plasma sources that have different features, HELCAT is capable of addressing various plasma phenomena in the same machine [1].

In this paper, the attention is focused on the control of the turbulence-driven particle transport in HELCAT. The control elements in HELCAT are a set of biased concentric ring electrodes that terminate the plasma column. It has been shown that by varying the bias of these ring electrodes, it is possible to manipulate the resulting $E \times B$ flow profile (i.e., the poloidal or azimuthal flow, V_θ) [2]. The radial derivative of the azimuthal flow (i.e., the flow shear), has been shown effective in increasing or decreasing the drift wave turbulence at the plasma edge. Hence, the turbulent fluctuations may be controlled indirectly in HELCAT by controlling the azimuthal flow profile evolution, $V_\theta(r, t)$.

Both open-loop and closed-loop approaches could control the azimuthal flow in HELCAT. So far, we have focused on an open loop control approach with the extremum seeking algorithm, which is shown effective for both fluctuation mitigation [3] and azimuthal flow regulation [4]. The main advantage of the open-loop approach is the possibility of utilizing highly complex transport models because the controller is computed off-line. On the other hand, the main drawback of the open-loop approach is that it is highly sensitive to disturbances and modeling uncertainties.

In this paper, a closed-loop approach based on the linear-quadratic-integral (LQI) optimal control theory is proposed. The proposed closed-loop controller is capable of coping with various model uncertainties as well as rejecting a nonlinear disturbance affecting the azimuthal flow profile, $V_\theta(r, t)$, dynamics. As the closed-loop control must be computed on-line, a reduced-order, control-oriented model is also proposed to replace the highly complex TransportHelicon code under development for HELCAT. The effectiveness of the proposed feedback controller is shown using numerical simulations.

The organization of this paper is as follows. The partial differential equation (PDE) model governing the azimuthal flow profile evolution in HELCAT is briefly introduced in Section II. This main model is reduced to a finite-dimensional, control-oriented model in Section III using the truncated Taylor series expansion method. The design of a LQI optimal feedback controller for the regulation of the azimuthal

Manuscript received August 8, 2013; revised December 20, 2013; accepted February 2, 2014. Date of current version March 6, 2014. This work was supported in part by the National Science Foundation under Grant PHY-0903803 and Grant PHY-0913663, and in part by the U.S. Department of Energy under Grant DE-FG02-09ER55022 and Grant DE-SC0001039.

Z. O. Ilhan, D. Huxley-Cohen, H. Wang, and E. Schuster are with the Department of Mechanical Engineering and Mechanics, Lehigh University, Bethlehem, PA 18015 USA (e-mail: zoi210@lehigh.edu; drh313@lehigh.edu; hew211@lehigh.edu; schuster@lehigh.edu).

M. Gilmore is with the Department of Electrical and Computer Engineering, University of New Mexico, Albuquerque, NM 87131 USA (e-mail: gilmore@ece.unm.edu).

A. Ware is with the Department of Physics and Astronomy, University of Montana, Missoula, MT 59812 USA (e-mail: andrew.ware@umontana.edu).

Color versions of one or more of the figures in this paper are available online at http://ieeexplore.ieee.org.

Digital Object Identifier 10.1109/TPS.2014.2304727

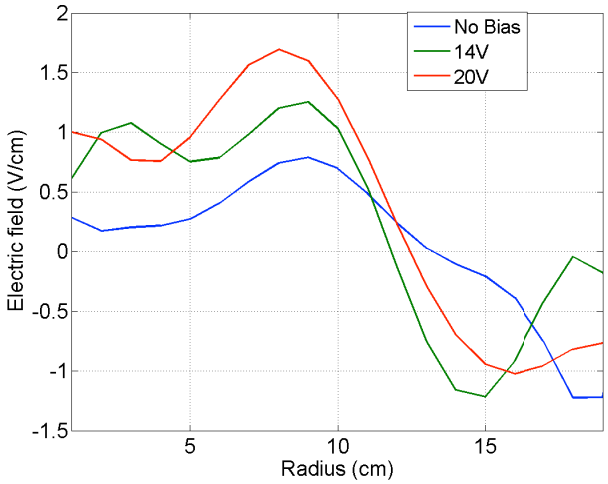

Fig. 1. E_r profiles as functions of the ring voltage bias (magnetic field $B = 352$ G), which show how the biasing affects E_r shear in HELCAT.

flow profile around a desired target profile is described in Section IV. In Section V, the proposed controller is then tested in simulations using the complete PDE model. Finally, conclusions and future work are stated in Section VI.

II. Azimuthal Flow Evolution Model

With [5], the radial-temporal evolution of the axially averaged azimuthal flow $V_\theta(\hat{r}, t)$ is governed by a PDE model ($t \geq 0$, $\hat{r} \in [0, 1]$) given by

$$\frac{\partial V_\theta}{\partial t} = S_\theta - \mu V_\theta + \frac{1}{\hat{r}}\frac{\partial}{\partial \hat{r}}\left[\hat{r} D_{V_\theta}\frac{\partial V_\theta}{\partial \hat{r}}\right] + \underbrace{\alpha_\theta \frac{\partial}{\partial \hat{r}}\left[\hat{r}^2 \epsilon \frac{\partial \epsilon}{\partial \hat{r}}\frac{\partial E_r}{\partial \hat{r}}\right]\left(\frac{2}{\hat{r}^2 f_{\text{ac}}}\right)}_{\textbf{Reynolds stress flow drive (nonlinear)}} \quad (1)$$

where $\hat{r}$ is the nondimensional plasma radius defined as $\hat{r} = r/a$, with r denoting the actual radius and $a \approx 15$ cm denoting the outer plasma radius. On the right-hand side (RHS) of (1), $S_\theta(\hat{r})$ is an external azimuthal flow (momentum) source, $D_{V_\theta}(\hat{r}, t)$ is the azimuthal flow diffusivity, $\epsilon(\hat{r}, t)$ is the plasma RMS fluctuation level, $E_r(\hat{r}, t)$ is the radial electric field profile, and $f_{\text{ac}}(\hat{r})$ is the Reynolds Stress suppression term. The model constants appearing on the RHS of (1) are the flow damping multiplier, μ, and the coefficient of Reynolds Stress flow generation, α_θ.

The control elements are the biased concentric rings in the actual HELCAT device. In HELCAT, as shown in Fig. 1, positive voltage biasing of the rings with respect to the grounded conducting wall can have clear and significant effects on the radial electric field profile, azimuthal velocity profile, fluctuation amplitudes, and turbulent radial flux. According to the work in [5], and as detailed in [4], the effect of the biased concentric rings is modeled as localized Gaussian momentum sources in the predictive transport code (TransportHelicon) that is under development for HELCAT. The effect will be identical to a source of poloidal $E \times B$ flow when diamagnetic flows are negligible [3]. Hence, the external azimuthal momentum source from the rings is modeled as

$$S_\theta(\hat{r}) = \sum_{j=1}^{6} p_c(j)\, e^{\frac{-(r_p(j)-\hat{r})^2}{2w_{pc}(j)^2}} \quad (2)$$

where the input array $p_c \in \mathbb{R}^{6\times 1}$ is the momentum source strengths, and the constant arrays $r_p \in \mathbb{R}^{6\times 1}$ and $w_{pc} \in \mathbb{R}^{6\times 1}$ are the radial locations and the radial widths of the Gaussian momentum sources, respectively.

On the RHS of (1), the diffusivity of the azimuthal velocity, $D_{V_\theta}(\hat{r}, t)$, is modeled as

$$D_{V_\theta}(\hat{r}, t) = 10D_0 + 50D_{0b}\sqrt{\frac{T_e}{\left|\frac{1}{T_e}\frac{\partial T_e}{\partial \hat{r}} + \frac{1}{n}\frac{\partial n}{\partial \hat{r}}\right|}}\,\epsilon^2\,\mu_{\text{prof}} \quad (3)$$

where the collisional particle transport coefficient D_0, the turbulent particle transport coefficient D_{0b}, and the turbulent transport profile modification μ_{prof} are all constants, and where $T_e(\hat{r}, t)$ and $n(\hat{r}, t)$ represent the plasma electron temperature and density profiles, respectively. Also, the Reynolds stress suppression term, f_{ac}, is defined as

$$f_{\text{ac}}(\hat{r}) = 1 + 10^{-6}\left[\frac{1}{(1.000001 - \hat{r})^6} + \frac{1}{(0.000001 + \hat{r})^6}\right]. \quad (4)$$

Note that the highly nonlinear last term appearing on the RHS of (1), denoted as $W(\hat{r}, t)$ in this paper, physically models the Reynolds stress flow drive. Hence, in the absence of the external momentum source effect (S_θ), the generation of flow is mainly a competition between the Reynolds stress flow drive [fourth term on the RHS of (1)] and both magnetic damping [second term on the RHS of (1)] and momentum diffusion [third term on the RHS of (1)].

III. Control-Oriented Model via Truncated Taylor Series

The nonlinear term associated with the Reynolds stress flow drive is bounded

$$\left|W(\hat{r}, t)\right| = \left|\alpha_\theta \frac{\partial}{\partial \hat{r}}\left[\hat{r}^2 \epsilon \frac{\partial \epsilon}{\partial \hat{r}}\frac{\partial E_r}{\partial \hat{r}}\right]\left(\frac{2}{\hat{r}^2 f_{\text{ac}}}\right)\right| \leq M. \quad (5)$$

Hence, from the control point of view, the Reynolds stress flow drive term is considered as a bounded nonlinear disturbance with an unknown upper bound, M. The disturbance-free azimuthal flow response model can then be represented by the following PDE:

$$\frac{\partial V_\theta}{\partial t} = S_\theta(\hat{r}) - \mu V_\theta + \frac{1}{\hat{r}}\frac{\partial}{\partial \hat{r}}\left(\hat{r} D_{V_\theta}(\hat{r}, t)\frac{\partial V_\theta}{\partial \hat{r}}\right) \quad (6)$$

with the imposed boundary conditions

$$\frac{\partial V_\theta}{\partial \hat{r}}(0, t) = 0, \quad V_\theta(1, t) = 0 \quad (7)$$

and a predefined initial condition

$$V_\theta(\hat{r}, 0) = V_{\theta_0}(\hat{r}). \quad (8)$$

The azimuthal flow diffusivity D_{V_θ} in (6) is both time and space dependent. Fig. 2(a) shows the radial profile of D_{V_θ} at different instants throughout the 250 ms discharge as extracted from the predictive TransportHelicon code for HELCAT.

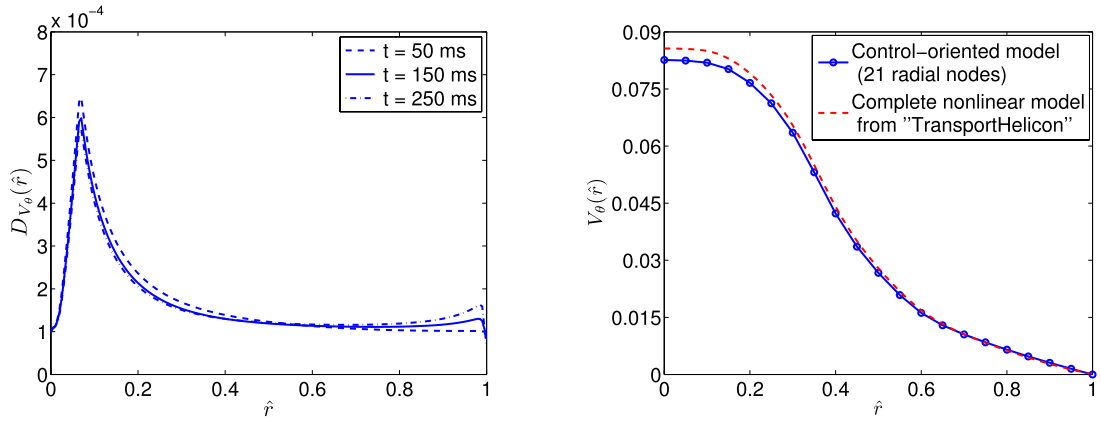

(a) (b)

Fig. 2. (a) Azimuthal flow diffusivity profiles extracted at different instants. (b) V_θ flow profiles at $t = 250$ ms for $p_c = [25, 10, 20, -10, 0, -5]$.

The profiles in Fig. 2(a) are similar in shape and do not vary much as time evolves. Hence, the profile at $t = 150$ ms can be used to approximate D_{V_θ} as a time-independent, radially varying term

$$D_{V_\theta}(\hat{r}, t) \approx \hat{D}_{V_\theta}(\hat{r}) = D_{V_\theta}(\hat{r}, t)\big|_{t=150\text{ms}}. \tag{9}$$

Using the approximation (9), the RHS of (6) can be expanded according to the chain rule as follows:

$$\frac{\partial V_\theta}{\partial t} = S_\theta - \mu V_\theta + \left(\frac{1}{\hat{r}}\hat{D}_{V_\theta} + \frac{\partial \hat{D}_{V_\theta}}{\partial \hat{r}}\right)\frac{\partial V_\theta}{\partial \hat{r}} + \hat{D}_{V_\theta}\frac{\partial^2 V_\theta}{\partial \hat{r}^2}. \tag{10}$$

To construct a reduced-order model suitable for control design, the governing PDE (10) is discretized in space using a truncated Taylor series expansion, which approximates the spatial derivatives while leaving the time domain continuous [6]. The nondimensional domain of interest, $\hat{r} \in [0, 1]$, can be divided into l nodes. Hence, the spacing between the nodes, h, becomes $h = 1/(l-1)$. The interior node region, $2 \le i \le (l-1)$, uses central finite difference spatial derivative approximations of $O(h^2)$. The left boundary node, $i = 1$, uses forward finite difference spatial derivative approximation of $O(h^2)$, and the right boundary node, $i = l$, is fixed by the Drichlet boundary condition imposed at $\hat{r} = 1$.

The infinite-dimensional azimuthal flow model (10) can then be discretized in space by using the aforementioned finite difference approximations together with the imposed boundary conditions (7). The resulting reduced-order, control-oriented model can be represented compactly in the standard linear, time-invariant, state-space form

$$\dot{x}(t) = \mathrm{A}x(t) + \mathrm{B}u(t) \tag{11}$$

where $x(t) = [V_{\theta_2}(t), V_{\theta_3}(t), \ldots, V_{\theta_{l-1}}(t)]^T \in \mathbb{R}^{n\times 1}$ is the state vector containing the values of $V_\theta(\hat{r}, t)$ at the $n = l-2$ interior nodes, the input vector $u(t) = [p_c(1), p_c(2), \ldots, p_c(6)]^T \in \mathbb{R}^{6\times 1}$ is the array of azimuthal momentum source strengths, $A \in \mathbb{R}^{n\times n}$ and $B \in \mathbb{R}^{n\times 6}$ are constant system matrices.

The elements of the state matrix A for the interior node $i = 2$ are given by

$$A_{1,1} = \frac{4}{3}\left[\frac{\hat{D}_2}{h^2} - \frac{1}{2h}\left(\frac{\hat{D}_2}{h} + \frac{\hat{D}_3 - \hat{D}_1}{2h}\right)\right] - \mu - 2\frac{\hat{D}_2}{h^2} \tag{12}$$

$$A_{1,2} = \frac{2}{3}\frac{\hat{D}_2}{h^2} + \frac{4}{3}\frac{1}{2h}\left(\frac{\hat{D}_2}{h} + \frac{\hat{D}_3 - \hat{D}_1}{2h}\right) \tag{13}$$

where $\hat{D}_i = \hat{D}_{V_\theta}(\hat{r}_i)$ is the discrete version of the radially varying, approximate diffusivity term, (9). Similarly, the elements of the A matrix for the interior region, $3 \le i \le (l-2)$, are given by

$$A_{i-1,i-2} = \frac{\hat{D}_i}{h^2} - \frac{1}{2h}\left(\frac{\hat{D}_i}{(i-1)h} + \frac{\hat{D}_{i+1} - \hat{D}_{i-1}}{2h}\right) \tag{14}$$

$$A_{i-1,i-1} = -\mu - 2\frac{\hat{D}_i}{h^2} \tag{15}$$

$$A_{i-1,i} = \frac{\hat{D}_i}{h^2} + \frac{1}{2h}\left(\frac{\hat{D}_i}{(i-1)h} + \frac{\hat{D}_{i+1} - \hat{D}_{i-1}}{2h}\right). \tag{16}$$

The elements for the interior node $i = l-1$ are given by

$$A_{n,n-1} = \frac{\hat{D}_{l-2}}{h^2} - \frac{1}{2h}\left(\frac{\hat{D}_{l-2}}{(l-3)h} + \frac{\hat{D}_{l-1} - \hat{D}_{l-3}}{2h}\right) \tag{17}$$

$$A_{n,n} = -\mu - 2\frac{\hat{D}_{l-2}}{h^2}. \tag{18}$$

The remaining entries of the state matrix A are all zero. Since the values of V_θ at the boundary nodes $i = 1$ and $i = l$ are known from the boundary conditions, they are not considered as the states for the control-oriented model (11).

The input matrix B in (11) models the azimuthal flow source term, S_θ in (6). Hence, for l radial nodes, (i.e., $n = l-2$ states), the elements of $B \in \mathbb{R}^{n\times 6}$ are obtained directly from the discrete version of the source model (2) as

$$B_{j,k} = \exp\left\{-\frac{\left[r_p(k) - (j-1)h\right]^2}{2\left[w_{pc}(k)\right]^2}\right\} \tag{19}$$

where $j = 1, 2, \ldots, n$ and $k = 1, 2, \ldots, 6$. The reduced-order, linear state-space model (11) is generated for

$l = 21$ nodes, (i.e., $n = 19$ states) and then compared with the actual nonlinear PDE (1), which is simulated using the predictive TransportHelicon code for HELCAT. The radial V_θ flow profiles obtained from the two models are then compared in Fig. 2(b). Although the state-space model (11) does not account for the nonlinear Reynolds stress flow drive term, it captures the main dynamics of the overall nonlinear V_θ flow model and hence is useful for feedback control design.

Note that the complete V_θ flow model (1) combines the disturbance-free model (6) with the Reynolds stress flow drive, which is considered in this paper as a bounded, nonlinear disturbance acting on the reduced-order model (11). Hence, the finite-dimensional form of the complete V_θ flow model (1) can be put into the following state-space model:

$$\dot{x}(t) = Ax(t) + Bu(t) + w(t) \tag{20}$$

where the vector $w(t) = [W_2(t), W_3(t), \ldots, W_{l-1}(t)]^T \in \mathbb{R}^{n\times 1}$ lists the value of the unknown but bounded disturbance, $W(r, t)$ at the $n = l - 2$ interior nodes.

IV. Controller Synthesis

A. Optimal Tracking Control Problem Statement

In addition to the state equation (20), an output equation can be defined to provide a linear combination of the states. The overall plant is then characterized by the following multi-input, multi-output (MIMO) system:

$$\dot{x}(t) = Ax(t) + Bu(t) + w(t) \tag{21}$$

$$y(t) = Cx(t) \tag{22}$$

where $C \in \mathbb{R}^{m\times n}$ is the output matrix and $y(t) \in \mathbb{R}^{m\times 1}$ is the output vector. The control objective is to make the output $y(t)$ track a constant reference z as closely as possible during the time interval $[0, t_f]$ with minimum control effort. Hence, for this application, the tracking error, $e(t) \in \mathbb{R}^{m\times 1}$, is defined as

$$e(t) = y(t) - z = Cx(t) - z. \tag{23}$$

The role of the matrix C is to select those states, that is, those spatial points of the azimuthal flow profile, that must track the constant reference values defined by the vector $z \in \mathbb{R}^{m\times 1}$. Hence, each row of C has only one nonzero element, which is equal to one and is located at the column associated with the state to be controlled. Thus, the output vector $y(t)$ returns m out of n states, whose reference values are given by the z vector.

To minimize a weighted combination of the tracking error and control energy, one can consider the standard, quadratic performance index

$$\min_{u(t)} J = \frac{1}{2}e^T(t_f)P(t_f)e(t_f) + \frac{1}{2}\int_0^{t_f}\left[e^T(t)Qe(t) + u^T(t)Ru(t)\right]dt \tag{24}$$

where $Q \in \mathbb{R}^{m\times m}$ and $R \in \mathbb{R}^{m\times m}$ are symmetric, positive definite matrices, and $P(t_f) \in \mathbb{R}^{m\times m}$. The disturbance-free plant

$$\dot{x}(t) = Ax(t) + Bu(t) \tag{25}$$

$$y(t) = Cx(t) \tag{26}$$

together with (23) and (24) define a standard linear-quadratic-tracking (LQT) optimal control problem, the solution of which is in state-feedback form utilizing the time-varying Kalman Gain [7]. However, the resulting system will produce some offset error while tracking the constant reference. To improve the tracking performance of the closed-loop system and reject the effect of the disturbance, integral action should be added to the optimal control law.

B. LQI Optimal Controller

The LQI optimal controller is considered here because it adds integral action to the standard LQT problem described in the previous section. Owing to the added integral action, the resulting closed-loop system will be capable of rejecting constant (or slowly varying, in practice) unknown process disturbance while tracking a constant reference. To obtain the LQI controller, which is also designed based on the disturbance-free model (25) and (26), the quadratic performance index (24) is modified as

$$\min_{v(t)} J = \frac{1}{2}e^T(t_f)P(t_f)e(t_f) + \frac{1}{2}\int_0^{t_f}\left[e^T(t)\mathrm{Q}e(t) + v^T(t)\mathrm{R}v(t)\right]dt \tag{27}$$

where $v(t)$ is the time derivative of the actual control input $u(t)$

$$v(t) = \frac{du(t)}{dt}. \tag{28}$$

Also, the augmented state vector $\tilde{x}(t) \in \mathbb{R}^{m+n}$ is introduced

$$\widetilde{x}(t) = \begin{bmatrix} e(t) \\ \cdots \\ x(t) \end{bmatrix}. \tag{29}$$

Differentiating (23)

$$\dot{e}(t) = C\dot{x}(t). \tag{30}$$

Similarly, from (25) and (28)

$$\ddot{x}(t) = A\dot{x}(t) + B\frac{du(t)}{dt} = A\dot{x}(t) + Bv(t). \tag{31}$$

Substituting (30) and (31) into (29), the time derivative of the augmented state vector, $\tilde{x}(t)$, becomes

$$\frac{d\widetilde{x}(t)}{dt} = \frac{d}{dt}\begin{bmatrix} e(t) \\ \dot{x}(t) \end{bmatrix} = \begin{bmatrix} 0 & C \\ 0 & A \end{bmatrix}\begin{bmatrix} e(t) \\ \dot{x}(t) \end{bmatrix} + \begin{bmatrix} 0 \\ B \end{bmatrix}v(t). \tag{32}$$

With (32), augmented matrices can be defined as

$$\widetilde{A} = \begin{bmatrix} 0_{m\times m} & C_{m\times n} \\ 0_{n\times m} & A_{n\times n} \end{bmatrix}, \quad \widetilde{B} = \begin{bmatrix} 0_{m\times m} \\ B_{n\times m} \end{bmatrix}. \tag{33}$$

Hence, the state equation for the enlarged $m + n$ dimensional system (32) can be rewritten as

$$\frac{d\widetilde{x}(t)}{dt} = \widetilde{A}\widetilde{x}(t) + \widetilde{B}v(t). \tag{34}$$

Note also that the performance index (27) can be expressed in terms of the enlarged system (34) as

$$\min_{v(t)} J = \frac{1}{2}\widetilde{x}^T(t_f)\widetilde{P}(t_f)\widetilde{x}(t_f) + \frac{1}{2}\int_0^{t_f}\left[\widetilde{x}^T(t)\widetilde{Q}\widetilde{x}(t) + v^T(t)Rv(t)\right]dt \tag{35}$$

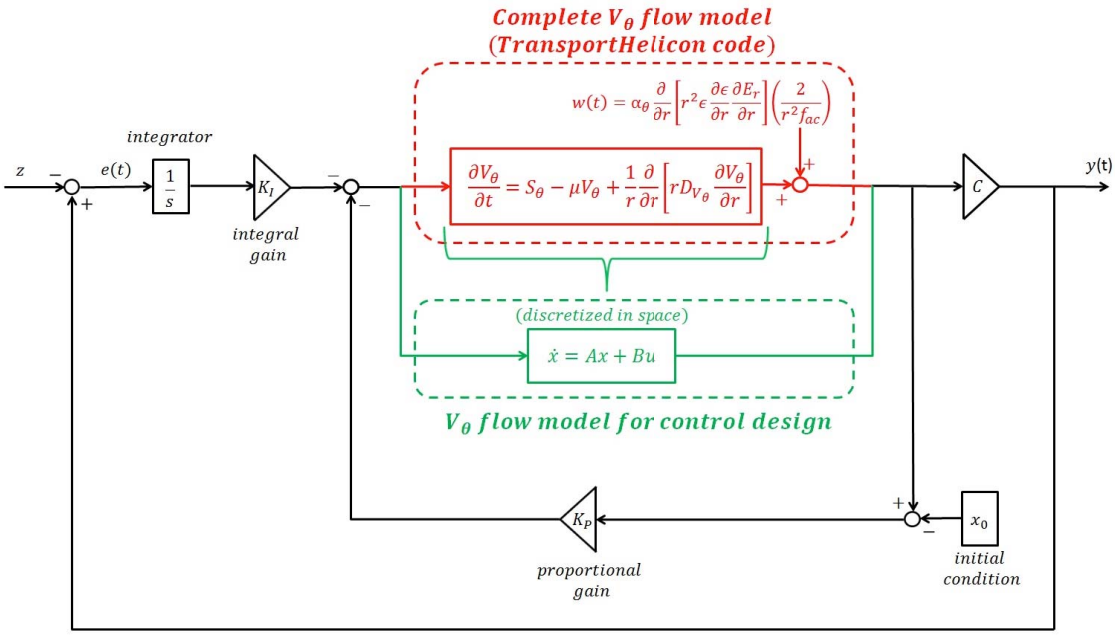

Fig. 3. Closed-loop control scheme implemented in the predictive transport code to test the performance of the designed LQI controller.

where the augmented weight matrices are

$$\widetilde{P}(t_f) = \begin{bmatrix} P_{m\times m} & 0_{m\times n} \\ 0_{n\times m} & 0_{n\times n} \end{bmatrix}, \quad \widetilde{Q} = \begin{bmatrix} Q_{m\times m} & 0_{m\times n} \\ 0_{n\times m} & 0_{n\times n} \end{bmatrix}. \tag{36}$$

Note that (34) and (35) define a standard linear-quadratic-regulator (LQR) problem, the solution of which yields a time-variant state-feedback of the form

$$v(t) = -K(t)\widetilde{x}(t) \tag{37}$$

where $K(t) \in \mathbb{R}^{m\times(m+n)}$ is the Kalman Gain given by

$$K(t) = R^{-1}\widetilde{B}^T\widetilde{P}(t) \tag{38}$$

and $\widetilde{P}(t)$ is the solution of the matrix Ricatti differential equation (RDE)

$$-\dot{\widetilde{P}}(t) = \widetilde{A}^T\widetilde{P}(t) + \widetilde{P}(t)\widetilde{A} - \widetilde{P}(t)\widetilde{B}R^{-1}\widetilde{B}^T\widetilde{P}(t) + \widetilde{Q} \tag{39}$$

subject to the final condition $\widetilde{P}(t_f)$ [7]. If the controllability and observability conditions are satisfied for $(\widetilde{A}, \widetilde{B})$ and $(\widetilde{A}, \widetilde{Q}^{1/2})$, respectively, then for every choice of $\widetilde{P}(t_f)$, there exists a constant, stationary matrix $\widetilde{P}_+$ that satisfies the RDE (39) in the limit as $t \to 0$. Furthermore, $\widetilde{P}_+$ is the unique positive definite solution to the algebraic Ricatti equation (ARE)

$$0 = \widetilde{A}^T\widetilde{P}_+ + \widetilde{P}_+\widetilde{A} - \widetilde{P}_+\widetilde{B}R^{-1}\widetilde{B}^T\widetilde{P}_+ + \widetilde{Q}. \tag{40}$$

In this case, the time-variant Kalman Gain (38) can be approximated by the constant gain K, which is given by

$$\begin{aligned} K &= R^{-1}\widetilde{B}^T\widetilde{P}_+ \\ &= [K_I \quad K_P] \\ &= \left[R^{-1}B^T\widetilde{P}_{21} \quad R^{-1}B^T\widetilde{P}_{22}\right] \end{aligned} \tag{41}$$

where $\widetilde{P}_{21} \in \mathbb{R}^{n\times m}$ and $\widetilde{P}_{22} \in \mathbb{R}^{n\times n}$ are partitions of $\widetilde{P}_+ \in \mathbb{R}^{(m+n)\times(m+n)}$ given by

$$\widetilde{P}_+ = \begin{bmatrix} \widetilde{P}_{11} & \widetilde{P}_{12} \\ \widetilde{P}_{21} & \widetilde{P}_{22} \end{bmatrix}. \tag{42}$$

Note from (41) that the first element of the K matrix, that is, $K_I \in \mathbb{R}^{m\times m}$ represents the integral gain and the second element, $K_P \in \mathbb{R}^{m\times n}$ gives the proportional state feedback gain. Using the constant gain K in (37), the optimal feedback control law $v(t)$ for the enlarged system (34) becomes

$$\begin{aligned} v(t) = -K\widetilde{x}(t) &= -[K_I \quad K_P]\begin{bmatrix} e(t) \\ \dot{x}(t) \end{bmatrix} \\ &= -K_I e(t) - K_P\dot{x}(t). \end{aligned} \tag{43}$$

Integrating (43) from the initial time $t = 0$ to any time t, the optimal feedback control law, $u(t)$, for the actual system (21) and (22) can be expressed as

$$u(t) = -K_I\int_0^t e(\tau)d\tau - K_P[x(t) - x_0] \tag{44}$$

where $x_0 = x(t = 0)$ is the initial condition for the state vector and the constant control gains are

$$K_I = R^{-1}B^T\widetilde{P}_{21} \quad K_P = R^{-1}B^T\widetilde{P}_{22}. \tag{45}$$

Finally, substituting the tracking error, $e(t)$, [i.e., (23)] back into (44), the optimal LQI feedback control law can be expressed in terms of the state and reference as

$$u(t) = -K_I\int_0^t [Cx(\tau) - z]\,d\tau - K_P[x(t) - x_0]. \tag{46}$$

Note that the optimal solution (46) yields a proportional plus integral (PI) control law.

V. Simulation Study

For $l = 21$ radial nodes, (i.e., $n = 19$ states), the controllability and observability conditions discussed in the previous section are satisfied when setting $m = 6$. In this way, the MIMO model [(21) and (22)] becomes perfectly square, having same number of inputs and outputs.

The constant weight matrices of the LQI performance index (27) are defined as $Q = 100\,I_{6\times6}$, and $R = 0.001\,I_{6\times6}$,

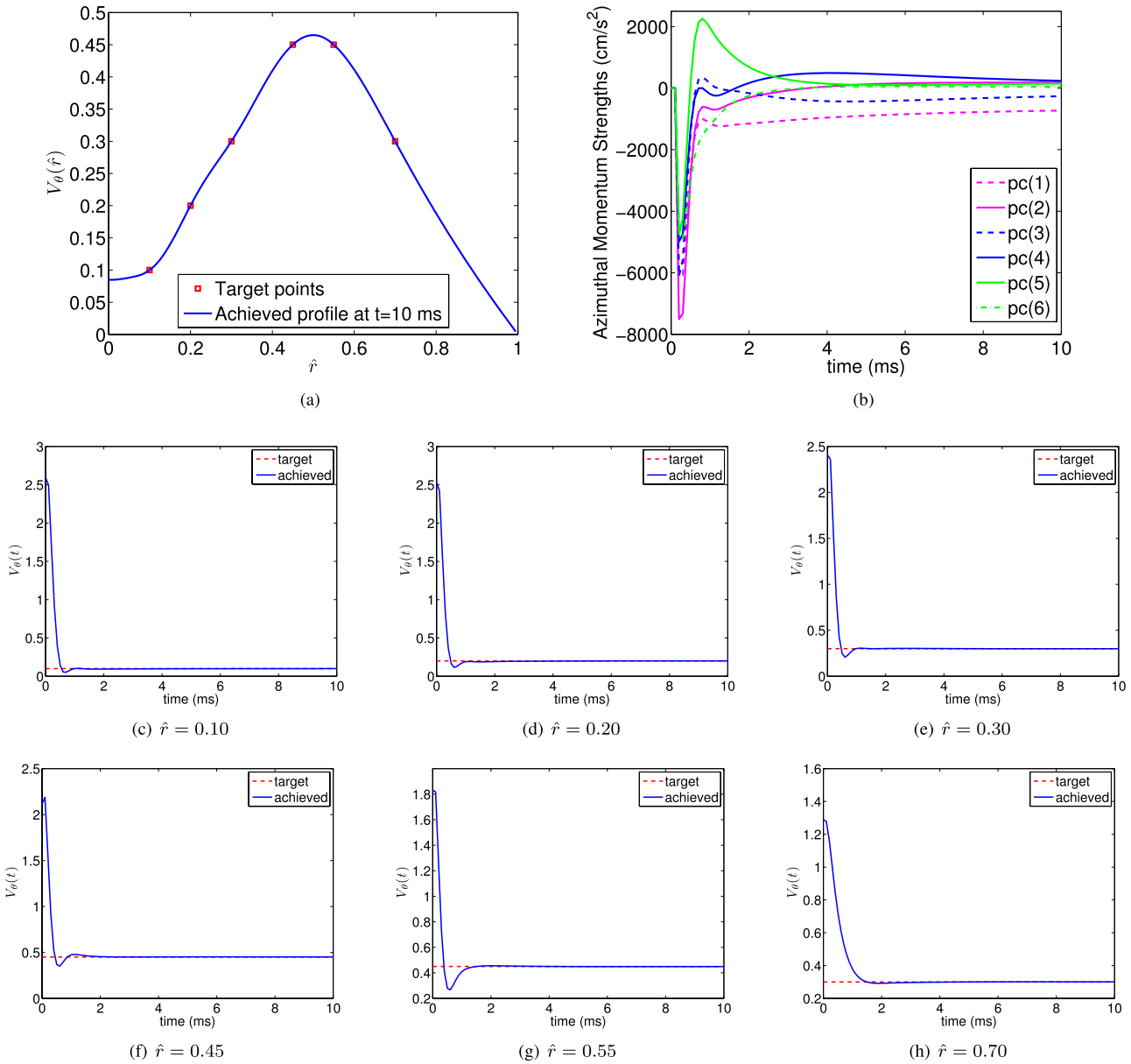

(a) (b)

(c) $\hat{r} = 0.10$ (d) $\hat{r} = 0.20$ (e) $\hat{r} = 0.30$

(f) $\hat{r} = 0.45$ (g) $\hat{r} = 0.55$ (h) $\hat{r} = 0.70$

Fig. 4. Results of the first reference tracking simulation study. (a) Comparison of the target points and the achieved $V_\theta(\hat{r})$ flow profile at $t_f = 10$ ms. (b) Time evolution of the optimal inputs. (c)–(h) Time evolutions of the outputs together with their respective target values for $\hat{r} = 0.10$, $\hat{r} = 0.20$, $\hat{r} = 0.30$, $\hat{r} = 0.45$, $\hat{r} = 0.55$, and $\hat{r} = 0.70$, respectively.

where I is the identity matrix. These values for the weight matrices indicate that in this paper the focus has been put on minimizing the tracking error at the expense of a larger control effort. The final value of the time-dependent matrix, $P(t_f) \in \mathbb{R}^{6\times 6}$, is taken as zero in this design. The ARE equation (40) is solved to obtain the proportional and integral control gains, K_p and K_I. The closed-loop LQI control scheme used for the simulation study is shown in Fig. 3. Note that while the control gains are designed based on the reduced-order, control-oriented model (11), which excludes the nonlinear Reynolds stress flow drive $W(\hat{r}, t)$, the simulation study is carried out based on the full predictive transport code TransportHelicon, which models not only the azimuthal velocity $V_\theta(\hat{r}, t)$ (1) but also the density $n(\hat{r}, t)$, electron temperature $T_e(\hat{r}, t)$, ion temperature $T_i(\hat{r}, t)$, axial velocity $V_z(\hat{r}, t)$, radial electric field $E_r(\hat{r}, t)$, and RMS fluctuation $\epsilon(\hat{r}, t)$. Therefore, during the control design process the loop is closed by the simplified, disturbance-free, state-space, plant model (lower block shown in green in Fig. 3), whereas during the control simulation tests the loop is closed by the full transport code (upper block shown in red in Fig. 3).

Because of controllability constraints, only 6 out of the 19 states can be forced to track a constant reference. Hence, one can achieve V_θ flow control only at six points along the plasma radius. Figs. 4 and 5 summarize the results of two simulation studies where different reference profiles are tracked. Both simulations are carried out from $t_0 = 0$ ms up to $t_f = 10$ ms. The red squares in Figs. 4(a) and 5(a) show the six radial locations where profile control is achieved. Given a desired profile shape, one can pick those six locations carefully so that the resulting profile approaches the target profile as closely as possible. One can force different states (radial locations) to track the reference by adequately specifying the nonzero entries in the output matrix, C, in (22).

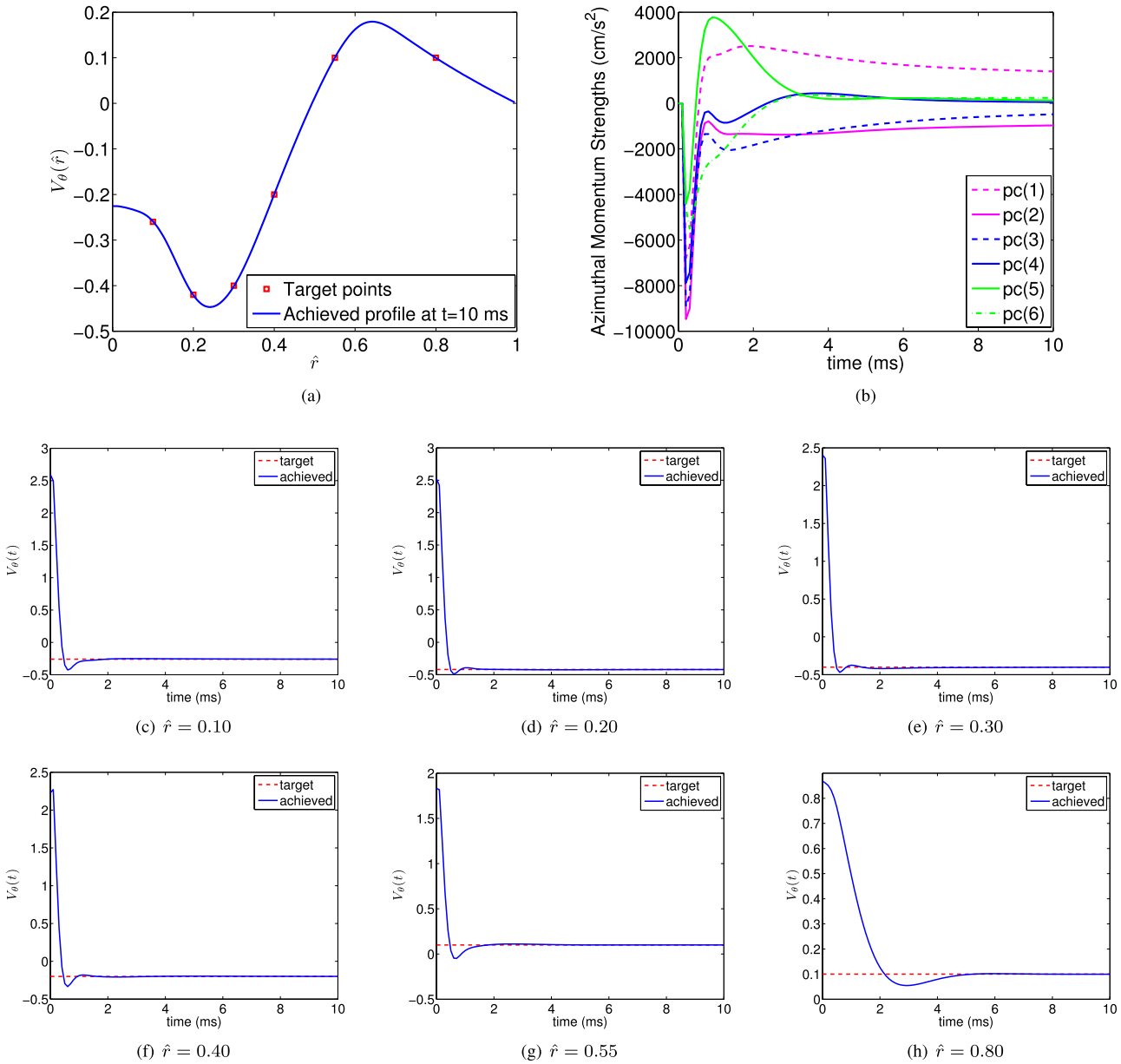

(a) (b)

(c) $\hat{r} = 0.10$ (d) $\hat{r} = 0.20$ (e) $\hat{r} = 0.30$

(f) $\hat{r} = 0.40$ (g) $\hat{r} = 0.55$ (h) $\hat{r} = 0.80$

Fig. 5. Results of the second reference tracking simulation study. (a) Comparison of the target points and the achieved $V_\theta(\hat{r})$ flow profile at $t_f = 10$ ms. (b) Time evolution of the optimal inputs. (c)–(h) Time evolutions of the outputs together with their respective target values for $\hat{r} = 0.10$, $\hat{r} = 0.20$, $\hat{r} = 0.30$, $\hat{r} = 0.4$, $\hat{r} = 0.55$, and $\hat{r} = 0.80$, respectively.

As can be seen from Figs. 4(b) and 5(b), the six optimal inputs (i.e., the azimuthal momentum source strengths) are settling down within the first few milliseconds of the discharge, regulating the outputs around their desired values, as shown in Figs. 4(c)–(h) and 5(c)–(h), respectively. It must be emphasized at this point that the settling time would be most likely longer if realistic saturation levels were imposed to the azimuthal momentum source strengths. However, the lack of a physical model connecting the biased ring voltages in the HELCAT device to the azimuthal momentum source strengths prevent at this moment the definition of realistic saturation levels.

VI. Conclusion

The PDE governing the dynamics of the azimuthal flow has been first discretized using a truncated Taylor series expansion to generate a control-oriented, linear model in cascade with an unknown but bounded disturbance. An LQI optimal controller has been then designed using the disturbance-free model. Numerical simulations based on a full transport predictive code show that the proposed controller is capable of tracking reference profiles while rejecting the bounded disturbance introduced by the effect of the Reynolds stress flow drive.

No restriction has been imposed so far on the actuators (momentum source strengths) in the predictive transport code or in the control design process as reflected by the choice of the weight matrices. One of the future goals is to develop a physical model converting the biased ring voltages in the HELCAT device to the azimuthal momentum source strengths in the transport code. Thus, the saturation of the actuators during both the control design and the control simulation could be considered because the voltage limits are well defined.

This would naturally lead to more realistic values for the azimuthal momentum strengths and azimuthal flows. The control synthesis approach proposed in this paper will remain valid and will be extended to the new set of control inputs (ring voltages).

The focus of this paper is on the control of transport on a transport time scale, and not fluctuations on much faster fluctuation time scales. As a consequence, the dynamic response model used for control synthesis simply averages over time the effect of fluctuations. Moreover, the focus of this paper has been 2-D in nature. Although the present experimental results in HELCAT suggest that axial dynamics will not drastically affect the transport control problem tackled in this paper, only experimental control tests in HELCAT will dictate how robust the control solution is against unmodeled axial dynamics, and eventually what type of axial phenomena need to be captured by the dynamic response model used for control synthesis.

A multipoint probe capable of simultaneously measuring the azimuthal flow at various points along the plasma is currently under development. This probe will be useful in determining target azimuthal flow profiles corresponding to low levels of RMS fluctuations and will also enable the implementation of the designed LQI controller in the actual HELCAT device.

REFERENCES

[1] A. G. Lynn, M. Gilmore, C. Watts, J. Herrea, R. Kelly, S. Will, *et al.*, "The HelCat dual-source plasma device," *Rev. Sci. Instrum.*, vol. 80, no. 10, pp. 103501-1–103501-8, Oct. 2009.

[2] N. Crocker, G. Y. Burin, M. J. Burin, G. R. Tynan, B. P. Cluggish, and K. R. Umstadter, "Control of velocity shear and turbulence through biasing in CSDX," in *Proc. 44th Annu. Meeting APS Division Plasma Phys.*, vol. 47. 2002, p. 264.

[3] Q. Wang, E. Schuster, M. Gilmore, S. Xie, and A. Ware, "Extremum-seeking-based fluctuation mitigation by E×B actuation in HELCAT," in *Proc. IEEE CCA*, Sep. 2011, pp. 301–306.

[4] Z. O. Ilhan, J. Barry, H. Wang, E. Schuster, M. Gilmore, and A. Ware, "Fluctuation mitigation and azimuthal velocity profile regulation by extremum seeking in HELCAT," in *Proc. IEEE 25th Symp. Fusion Eng.*, Jun. 2013, pp. 1–6.

[5] D. E. Newman, B. A. Carreras, D. Lopez-Bruna, P. H. Diamond, and V. B. Lebedev, "Dynamics and control of internal transport barriers in reversed shear discharges," *Phys. Plasmas*, vol. 5, no. 4, pp. 938–952, Jan. 1998.

[6] W. Schiesser, *The Numerical Method of Lines: Integration of Partial Differential Equations*. San Diego, CA, USA: Academic, 1991.

[7] D. Naidu, *Optimal Control Systems*. Boca Raton, FL, USA: CRC Press, 2003.

Zeki Okan Ilhan received the B.Sc. degree in mechanical engineering from Middle East Technical University, Ankara, Turkey, in 2010. He is currently pursuing the Ph.D. degree in mechanical engineering and mechanics from Lehigh University, Bethlehem, PA, USA.

He is a member of the Lehigh University Plasma Control Group within the Laboratory for Control of Complex Physical Systems.

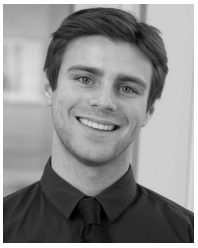

David Huxley-Cohen received the B.Sc. degree in mechanical engineering and environmental sustainability from Lehigh's Integrated Degree in Engineering and Arts and Science honors program, Lehigh University, Bethlehem, PA, USA, in 2013. He is currently pursuing the M.Sc. degree from the Energy Systems Engineering program, Lehigh University.

He was with the Lehigh University Plasma Control Group supported by the National Science Foundation Research Experience for Undergraduates program. He is currently a Presidential Scholar.

Hexiang Wang received the B.Sc. and M.Sc. degrees in mechanical engineering from the East China University of Science and Technology, Shanghai, China, and the University of Manchester, Manchester, U.K., in 2009 and 2011, respectively. He is currently pursuing the M.Sc. degree in mechanical engineering and mechanics from Lehigh University, Bethlehem, PA, USA.

He is a member of the Lehigh University Plasma Control Group within the Laboratory for Control of Complex Physical Systems.

Eugenio Schuster received the B.Sc. degrees in electronic engineering from the University of Buenos Aires, Buenos Aires, Argentina, and nuclear engineering from the Balseiro Institute, San Carlos de Bariloche, Argentina, and the M.Sc. and Ph.D. degrees in mechanical and aerospace engineering from the University of California at San Diego, San Diego, CA, USA, in 1993, 1998, 2000, and 2004, respectively.

He is an Associate Professor with the Department of Mechanical Engineering and Mechanics, Lehigh University, Bethlehem, PA, USA. He is the Director of the Laboratory for Control of Complex Physical Systems and the Head of the Lehigh University Plasma Control Group. His current research interests include distributed-parameter and nonlinear control of nuclear-fusion plasmas.

Prof. Schuster is the recipient of the NSF Career Award.

Mark Gilmore received the B.Sc. degree in electrical engineering from Boston University, Boston, MA, USA, the M.Sc. degree in electrical engineering from Northeastern University, Boston, and the Ph.D. degree in electrical engineering from the University of California, Los Angeles, CA, USA, in 1999.

He is an Associate Professor with the Department of Electrical and Computer Engineering, University of New Mexico, Albuquerque, NM, USA.

Prof. Gilmore serves as the Senior Editor for diagnostics for the IEEE TRANSACTIONS ON PLASMA SCIENCE. He has been involved in a wide variety of areas within plasma science, including basic physics of turbulence and transport in both laboratory and magnetic fusion plasmas. He has served on the Plasma Science and Applications Executive Committee of the IEEE NPSS, and on the executive committee of the University Fusion Association.

Andrew Ware received the B.S. degree in physics from the University of Texas, Austin, TX, USA, and the Ph.D. degree in physics from the University of California at San Diego, CA, USA, in 1988 and 1992, respectively.

He is a Professor with the Department of Physics and Astronomy, University of Montana, Missoula, MT, USA. His current research interests include plasma turbulence, turbulent transport, and 3-D plasma equilibrium, stability, and transport.